Theory of the Benguela Upwelling System

WOLFGANG FENNEL

Institut für Ostseeforschung, Warnemünde (IOW), an der Universität Rostock, Rostock, Germany

(Manuscript received 30 July 1997, in final form 3 March 1998)

ABSTRACT

The paper gives a theoretical study of the Benguela upwelling system by means of a relatively simple conceptual model that allows an analytical treatment. The model consists of a stratified, flat-bottomed coastal ocean. The coast is idealized by a straight wall. The model ocean is forced by an alongshore wind band extending from the area near Cape Town to the border of Angola and Namibia. The wind varies alongshore and cross-shore (wind stress curl) and changes periodically in time.

The response of the coastal ocean is governed by coastal jets, upwelling, and Kelvin waves, as well as by a current system driven by the wind stress curl. The model is able to reproduce several observed features such as the poleward undercurrent, the northward coastal currents in most of the wind band, and a southward coastal current near the northern edge of the wind band.

Export of coastal jets out of the forcing area by coastal Kelvin waves provide a mechanism to guide energy into the area off Cape Town. The southward propagating Kelvin waves may bend around the southern tip of Africa and provide a dynamic linkage between the Benguela coastal current and the Agulhas Current.

1. Introduction

The Benguela Current is a broad northward flow off southwestern Africa and is part of the South Atlantic subtropical gyre. It is driven by large-scale wind patterns and thermohaline forcing (Garzoli and Gordon 1996). The currents close to the coast are known as the Benguela upwelling system, which is forced locally by the wind stress field off Southwest Africa (Nelson and Hutchings 1983). General descriptions of the Benguela upwelling system are given, for example, in the review articles of Shannon (1985) and Shannon and Nelson (1996).

The Benguela upwelling system stretches from the southern tip of Africa to about 15°–16°S where it is bounded by the Angola front, which separates the warm water of the Angola Current from the cold Benguela water. A schematic of the Benguela, which was redrawn after Nelson and Hutchings (1983), Shannon (1985), and Shannon and Nelson (1996), is shown in Fig. 1. In the northern part of the Benguela upwelling system a poleward surface flow is found that extends as far south as 17°–18°S. Yamagata and Iizuka (1995) found some indications that coastal Kelvin waves, which originate from equatorial Kelvin waves, carry downwelling southward. These waves might be a possible reason for the occurrence of a poleward flow south of the Angola front. The upwelling varies alongshore. The strongest signals are found off Lüderitz, Namibia (Shannon 1985).

The area of the Benguela is exposed to a persistent alongshore wind associated with the St. Helena high pressure system. The upwelling favorable alongshore wind has a maximum at about 25°S and decreases toward the northern and southern boundaries of the Benguela system at the Angola front and the southern tip of Africa, respectively. In the south the winds are highly seasonal and reach a maximum during spring and summer (Boyd 1987; Shannon and Nelson 1996). North of 31°S the seasonal variation is weaker with permanent alongshore winds with a spring–summer maximum and autumn minimum as far north as 25°S. North of that latitude the maximum occurs in late winter to spring. The wind increases somewhat away from the coast. This manifests in wind stress curl, as discussed in Bakun and Nelson (1991) and Shannon and Nelson (1996).

As a simple model of the Benguela upwelling system we consider a coastal ocean, with a north–south oriented coast, forced by a band of alongshore wind with a bell-shaped alongshore structure and a gradual increase of the wind with increasing distance from the coast. The time behavior of the wind can be described roughly by a small seasonal cycle added to a constant wind. Important features of the eastern boundary upwelling systems can be illuminated by analytically tractable linear models that describe the response of a coastal f-plane

Corresponding author address: Prof. Wolfgang Fennel, Institut für Ostseeforschung Warnemünde, an der Universität Rostock, P.O. Box 30 10 38, D-18119 Rostock, Germany.
E-mail: wolfgang.fennel@io-warhemuende.de

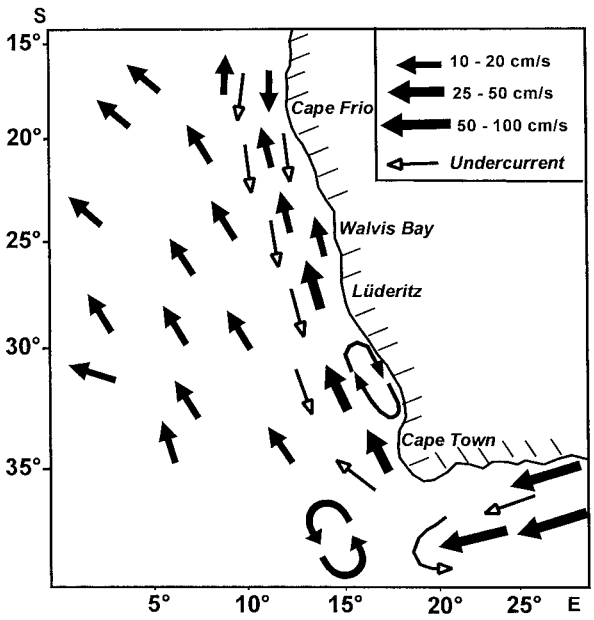

FIG. 1. A schematic of the surface flow and undercurrent in the Benguela region, redrawn after Nelson and Hutchings (1983), Shannon (1985), and Shannon and Nelson (1996).

ocean to a band of constant alongshore wind (e.g., McCreary 1981; Fennel 1988).

For an inviscid coastal ocean we have the following scenario: After a sudden onset of the wind, an accelerating coastally trapped downwind jet associated with coastal upwelling develops inside the wind band. At the northern edge of the band, Kelvin waves are generated, which propagate with the coast to the left in the Southern Hemisphere. The Kelvin waves arrest the coastal jet, stop the upwelling, and establish an undercurrent. At the southern edge the Kelvin waves export the coastal surface jet, the upwelling, and the undercurrent into the unforced area outside the wind band. Thus, after a spin-up time, which is set by the time the coastal Kelvin waves need to cross the wind band, the upwelling ceases. This implies that only temporal variations of the alongshore wind can excite new events of upwelling and downwelling. This simple picture is significantly modified if friction is included because then the travelling distance of the Kelvin waves is limited. Additional features emerge if spatial variations of the wind field are involved.

In this paper we develop an analytically tractable theory that includes the cross- and alongshore structures of the wind field and takes the annual cycle of the wind into account. Cross-boundary wind variations, or equivalently wind stress curl, drive Ekman divergences and provide an additional source of upwelling as well as downwind flows and countercurrents. Such flow patterns are, for example, known in marginal ice zones near ice edges (e.g., Fennel and Johannessen 1997). The role of a wind-stress curl near a coastal boundary was discussed by McCreary et al. (1987) to explain the occurrence of a coastal flow against the local wind off California.

In the Benguela system the existence of southward propagating Kelvin waves would imply an export of energy outside the forcing area. The Kelvin waves can bend around the southern tip of Africa and drive a westward coastal flow along the southern coast, which may affect the Agulhas Current south of Africa. The Agulhas Current is the western boundary current of the southern Indian Ocean, being most intense along the east coast of southern Africa. South of Africa the Agulhas has features of a free inertial jet, which starts to meander and decays into eddies and rings in the Agulhas retroflection zone (see the review of Lutjeharms 1996).

There is some evidence of a certain dynamical linkage between the Benguela coastal flow and the Agulhas. Bang (1973) noted that nearly always vestiges of Agulhas water can be observed west of Cape Town. Schumann et al. (1982) and Shannon et al. (1983) showed that upwelling extends along the south coast as far as 25°E. In 1986 an intrusion of waters with the signature of the Agulhas into the Benguela was observed (Shannon et al. 1990).

In this paper the following questions are addressed:

1) What part is played by coastal Kelvin waves and by the wind stress curl in shaping the flows in the Benguela upwelling system?
2) Is the poleward surface flow, which extends roughly to Cape Frio at 17°–18°S, supported by wind stress curl?
3) Is there a dynamical linkage between the northward Benguela surface flow and the Agulhas Current?

The paper is arranged as follows. In section 2 the theory and the model are outlined. Section 3 decribes the analytical solution. A discussion of the results is given in section 4 and the paper concludes with a summary and conclusions in section 5.

2. The model ocean

a. The model

We consider an f-plane ocean with a flat bottom at depth H, bounded by a north–south oriented straight coast. We assume a band of alongshore, southerly wind field of the length $2a$, which roughly covers the area from Cape Town to the border of Angola and Namibia in the north. A schematic of the model is shown in Fig. 2. The wind band has a length of roughly 15°, which corresponds to 1650 km, that is, $a = 825$ km. We assume a depth of $H = 1$ km and choose the mean inertial frequency as $f(25°\text{S}) = 2\pi/1.2$ d. Moreover, we use for the first mode Rossby radius the value $R_1 = 55$ km, which is consistent with the global distribution of Rossby radii as discussed by Emery et al. (1984). Thus, the length of the wind band equals $30R_1$ and the barotropic

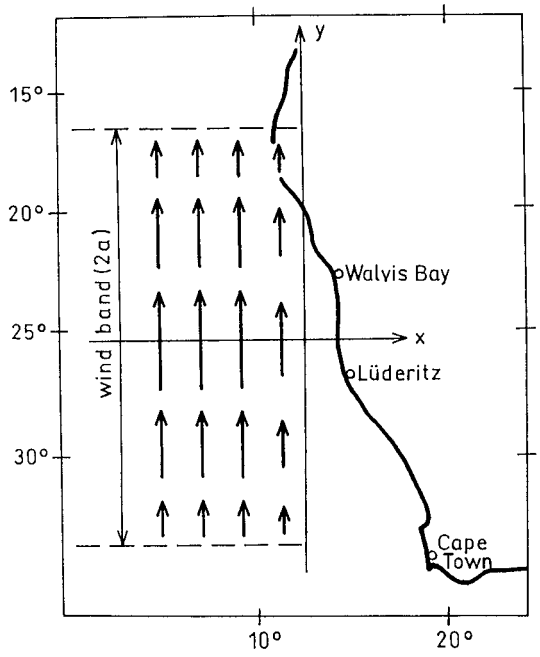

FIG. 2. A schematic of the simplified model of the eastern boundary of Southwest Africa.

Rossby radius is $R_0 = \sqrt{gH}/f = 30R_1$. The scale of the phase speed associated with the first baroclinic mode is $c_1 = fR_1 = 290$ km d^{-1}. A first mode baroclinic signal, which propagates with the phase speed c_1, would cross the wind band in 6 days.

b. Basic equations

The theory is based on the linear, hydrostatic Boussinesq equations for a flat-bottomed f-plane ocean in the Southern Hemisphere, bounded by a north–south oriented straight coast with vertical walls:

$$u_t + ru + fv + p_x = X, \tag{1}$$

$$v_t + rv - fu + p_y = Y, \tag{2}$$

$$p_{zt} + rp_z - N^2 w = 0, \tag{3}$$

$$u_x + v_y + w_z = 0. \tag{4}$$

Here u, v, and w are the cross-shore, alongshore, and vertical current components, respectively; p is the perturbation pressure divided by the density; f is the Coriolis parameter; r is a linear friction rate; N is the Brunt–Väisälä frequency; and X and Y are wind forces in the x and y direction. The coast is along the y axis, that is, $x = 0$. The subscripts x, y, z, and t refer to partial differentiation.

The boundary conditions on u and w are

$$u = 0 \quad \text{for } x = 0, \qquad |u| < \infty \quad \text{for } x \to -\infty \tag{5}$$

and

$$w = \frac{p_t}{g} \quad \text{for } z = 0, \qquad w = 0 \quad \text{for } z = -H. \tag{6}$$

The vertical coordinate z can be separated by expanding the dynamical quantities into a series of vertical eigenfunctions, $F_n(z)$,

$$\phi(x, y, z, t) = \sum_{n=0}^{\infty} \phi_n(x, y, t)F_n(z), \tag{7}$$

where ϕ stands for u, v, and p. The $F_n(z)$ are subject to the vertical eigenvalue problem,

$$\left(\frac{d}{dz}\frac{1}{N^2}\frac{d}{dz} + \lambda_n^2\right)F_n(z) = 0, \tag{8}$$

with the boundary conditions

$$F_n'(0) + \frac{N^2(0)}{g}F_n(0) = 0, \qquad F_n'(-H) = 0.$$

For a constant N we have $F_0 = 1/\sqrt{H}$, $\lambda_0 = 1/\sqrt{gH}$, and

$$F_n(z) = \sqrt{\frac{2}{H}}\cos\left(\frac{n\pi z}{H}\right),$$

$$\lambda_n = \frac{n\pi}{NH}, \qquad (n = 1, 2, \ldots).$$

Note that $c_n = 1/\lambda_n = c_1/n$ and $R_n = R_1/n$.

c. Formal solution

A formal solution of the response of the sea to the wind forcing is given by Fennel (1988). We use the Fourier transforms with respect to y and t,

$$\phi_n(x, y, t) = \int_{-\infty}^{\infty} \frac{d\kappa}{2\pi}\frac{d\omega}{2\pi} e^{i\kappa y - i\omega t}\phi_n(\kappa, \omega, x), \tag{9}$$

where ϕ stands for u, v, p, X, and Y. In the Fourier domain Eqs. (1), (2), and (4) have the form

$$-i\bar{\omega}u_n + fv_n + p_{nx} = X_n, \tag{10}$$

$$-i\bar{\omega}v_n - fu_n + i\kappa p_n = Y_n, \tag{11}$$

$$u_{nx} + i\kappa v_n - i\bar{\omega}\lambda_n^2 p_n = 0, \tag{12}$$

where $\bar{\omega} = \omega + ir$. An equation for u_n alone can easily be derived:

$$\frac{d^2}{dx^2}u_n(x) - \alpha_n^2 u_n(x) = \frac{i(\bar{\omega}^2\lambda_n^2 - \kappa^2)}{\bar{\omega}}X_n + \left(\lambda_n^2 f + \frac{\kappa}{\bar{\omega}}\frac{d}{dx}\right)Y_n, \tag{13}$$

where $\alpha_n^2 = \lambda_n^2(f^2 - \overline{\omega}^2) + \kappa^2$. Next we introduce a Green's function by means of

$$\frac{d^2}{dx^2}G_n(x; x') - \alpha_n^2 G_n(x; x') = \delta(x - x'), \quad (14)$$

with $\delta(x - x')$ being a Dirac function. The solution is

$$G_n(x; x') = \frac{1}{2\alpha_n}(e^{\alpha_n(x+x')} - e^{-\alpha_n|x-x'|}). \quad (15)$$

A formal solution for u_n can readily be obtained in terms of a source representation by combining (13) and (14) and using Green's theorem.

The formal solution is

$$u_n(x, \omega, \kappa) = \frac{i}{\overline{\omega}}(\overline{\omega}^2\lambda_n^2 - \kappa^2)G_n \cdot X_n + \lambda_n^2 f G_n \cdot Y_n + \frac{\kappa}{\overline{\omega}}G_n \cdot Y_{nx'}, \quad (16)$$

$$v_n(x, \omega, \kappa) = -f\lambda_n^2 G_n \cdot X_n + G_{nx} \cdot X_n + \frac{i}{\overline{\omega}^2\lambda_n^2 - \kappa^2}\left(\overline{\omega}\lambda_n^2 Y_n + \frac{\overline{\omega}\lambda_n^2}{R_n^2}G_{nx} \cdot Y_n + \kappa f\lambda_n^2 G_n \cdot Y_{nx'} - f\kappa\lambda_n^2 G_{nx} \cdot Y_n - \frac{\kappa^2}{\overline{\omega}}G_{nx} \cdot Y_{nx'}\right), \quad (17)$$

$$p_n(x, \omega, \kappa) = -\frac{\kappa}{\overline{\omega}}G_n \cdot X_n - G_{nx} \cdot X_n + \frac{i}{\overline{\omega}\lambda_n^2 - \kappa^2}\left(\kappa Y_n - \overline{\omega}\lambda^2 f G_{nx} \cdot Y_n - \kappa G_{nx} \cdot Y_{nx'} + \lambda^2 f\kappa G_{nx'} \cdot Y_n - \frac{\kappa^2}{\overline{\omega}}G_{nx} \cdot Y_{nx'}\right). \quad (18)$$

Expressions like $G_n \cdot Y_n$ stand for convolution integrals of the Green's function, G_n, and the forcing function Y_n:

$$G_n \cdot Y_n = \int_{-\infty}^{0} dx' G_n(x; x')Y_n(x'). \quad (19)$$

The set (16)–(18) gives the formal solution in the ω–κ domain. In order to find an explicit solution we have to specify the forcing functions.

d. Forcing function and parameter choices

The model is forced by an alongshore wind that varies in space and time. For simplicity we use a smoothly increasing and decreasing alongshore wind approaching zero values near the southern tip of Africa at about 30°S and in the north at the border of Angola at 15°S. We choose the positive half-wave of a cosine profile; that is,

$$Q(y) = \theta(a - |y|)\cos(\kappa_0 y), \quad (20)$$

with $\kappa_0 = \pi/(2a)$ where $2a$ is the length of the wind band. Here $\theta(x)$ is the step function ($\theta(x) = 1$ for $x > 0$ and $\theta(x) = 0$ for $x < 0$).

The yearly cycle is simulated by a sinusoidal variation added to a constant wind:

$$T(t) = 1 + f_{sc}\sin(\omega_0 t), \quad (21)$$

where f_{sc} controls the amplitude of the seasonal cycle and with $\omega_0 = 2\pi/366\ \text{d}^{-1}$. Moreover, it is assumed that the alongshore wind decreases toward the coast by about 25% within a strip of width l, which is assumed to be of the order of the first mode Rossby radius, R_1. We choose the cross-shore wind profile $\Pi(x)$ as

$$\Pi(x) = \Pi_\infty\theta(-x - l) + \theta(x + l)[\Pi_\infty - \gamma(x + l)], \quad (22)$$

where $\gamma = (\Pi_\infty - \Pi_0)/l$ determines the slope of the decrease of the wind toward the coast. We set $\Pi_\infty = 1$ and $\Pi_0 = 0.75$.

The maximum alongshore wind stress is assumed as $\tau^y = 1.2$ dyn cm^{-2}, which is equivalent to the friction velocity $v^2{}_* = 1.2$ cm^2 s^{-2}. This implies a maximum wind stress curl of 4.5×10^{-8} dyn cm^{-3}. This order of magnitude is consistent with the findings of Shannon and Nelson (1996), where the maps Bakun and Nelson (1991) are slightly modified.

The wind is considered to enter the ocean as a volume force evenly distributed over an upper mixed layer of thickness H_{mix}. The forcing has the analytical shape

$$Y(x, y, z, t) = \frac{v_*^2}{H_{mix}}\theta(z + H_{mix})T(t)Q(y)\Pi(x). \quad (23)$$

The seasonal cycle and spatial structure of the model wind are shown in Fig. 3. After Fourier transformation with respect to t and y and expansion into vertical modes we find

$$Y_n(x, \omega, \kappa) = \frac{v_*^2}{h_n}T(\omega)Q(\kappa)\Pi(x), \quad (24)$$

where

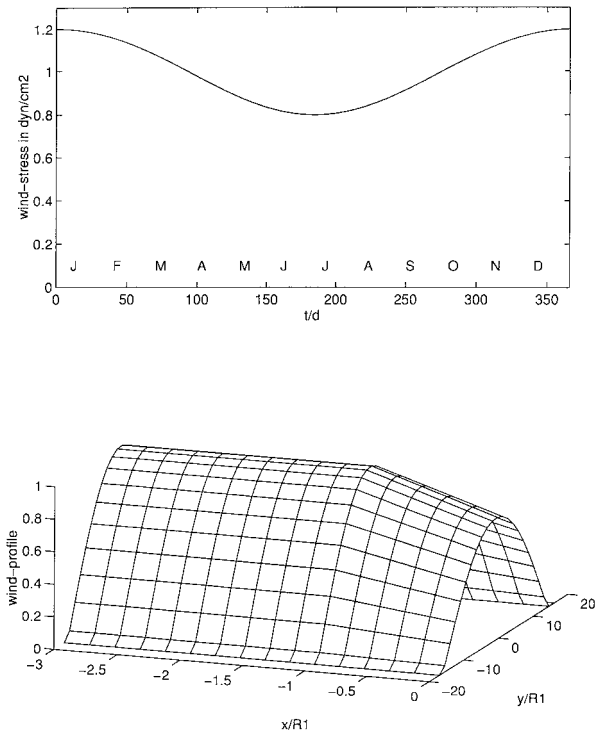

FIG. 3. The annual cycle (top) and the spatial structure (bottom) of the model wind.

$$\frac{1}{h_0} = \sqrt{\frac{1}{H}}; \qquad \frac{1}{h_n} = \sqrt{\frac{2}{H}} \frac{\sin\left(\frac{n\pi}{H} H_{\text{mix}}\right)}{\frac{n\pi}{H}} \quad \text{for } n \geq 1 \tag{25}$$

and

$$T(\omega) = 2\pi\delta(\omega) + f_{\text{sc}} \frac{\pi}{i} [\delta(\omega + \omega_0) - \delta(\omega - \omega_0)], \tag{26}$$

$$Q(\kappa) = \frac{\sin[a(\kappa + \kappa_0)]}{\kappa + \kappa_0} + \frac{\sin[a(\kappa - \kappa_0)]}{\kappa - \kappa_0}. \tag{27}$$

3. Calculation of the response

Inserting the forcing (24) into (16) to (18) gives the formal solution of our problem in Fourier space. Next we have to estimate the convolution integrals $G_n \cdot \Pi$, $G_n \cdot \Pi_{x'}$, and $G_{nx} \cdot \Pi$, which are defined by (19) in an obvious manner. The integration can easily be done if the properties of Green's function are used as described in the appendix. In the following we employ the long-wave approximation, $\kappa R_1 \ll 1$, and consider the low-frequency limit $\omega \ll f$, and $r \ll f$. Then we find

$$u_n(x, \omega, \kappa) = \frac{v_*^2}{f h_n} T(\omega) Q(\kappa) \left(-\Pi(x) + \Pi_0 e^{x/R_n} + \frac{\gamma R_n}{2} (e^{(x-l)/R_n} - e^{(-|x+l|)/R_n}) \right), \tag{28}$$

$$v_n(x, \omega, \kappa) = \frac{v_*^2}{h_n} T(\omega) Q(\kappa) i \left[\frac{\lambda_n}{\kappa + \overline{\omega}\lambda_n} \left(\Pi_0 e^{x/R_n} - \gamma R_n (e^{x/R_n} - e^{(x-l)/R_n}) + \frac{\gamma R_n}{2\overline{\omega}} (2e^{x/R_n} - e^{(x-l)/R_n} - e^{(-|x+l|)/R_n}) \right) \right], \tag{29}$$

$$p_n(x, \omega, \kappa) = \frac{v_*^2}{h_n} T(\omega) Q(\kappa) i \left\{ \frac{1}{\kappa + \overline{\omega}\lambda_n} \left[-\Pi_0 e^{x/R_n} + \gamma R_n (e^{x/R_n} - e^{(x-l)/R_n}) + \frac{f R_n^2}{\overline{\omega}} \left(\Pi_x(x) + \frac{\gamma}{2} (-2e^{x/R_n} + e^{(x-l)/R_n} - \text{sgn}(x + l) e^{(-|x+l|)/R_n}) \right) \right] \right\}. \tag{30}$$

The Fourier transforms with respect to κ amounts to the estimation of the integral

$$I_n(y, \overline{\omega}) = \int_{-\infty}^{\infty} \frac{d\kappa}{2\pi} \frac{Q(\kappa)}{\kappa + \overline{\omega}\lambda_n} e^{i\kappa y}, \tag{31}$$

which gives explicitly

$$I_n(y, \overline{\omega}) = \frac{1}{\overline{\omega}^2 \lambda_n^2 - \kappa_0^2} \Big(\overline{\omega}\lambda_n Q(y) + i\kappa_0 \langle \theta(a - y) \{ \exp[i\overline{\omega}\lambda_n (a - y)] - \sin(\kappa_0 y) \} + \theta(-a - y) \{ \exp[-i\overline{\omega}\lambda_n (a + y)] + \sin(\kappa_0 y) \} \rangle \Big). \tag{32}$$

The Fourier transformation with respect to ω involves the integrals

$$T_{\text{int}}(t) = \int_{-\infty}^{\infty} \frac{d\omega}{2\pi} i \frac{T(\omega)}{\overline{\omega}} e^{-i\omega t} = \frac{1}{r} + \frac{f_{\text{sc}}}{\omega_0^2 + r^2}[r \sin(\omega_0 t) - \omega_0 \cos(\omega_0 t)] \quad (33)$$

and

$$\Lambda_n(y, t) = \int_{-\infty}^{\infty} \frac{d\omega}{2\pi} iT(\omega) I_n(y, \overline{\omega}) e^{-i\omega t} = iI_n(y, ir) + \frac{f_{\text{sc}}}{2}[I_n(y, -\omega_0 + ir)e^{-i\omega_0 t} - I_n(y, \omega_0 + ir)e^{i\omega_0 t}]. \quad (34)$$

With (28)–(30) and (34) we find in the physical space

$$u_n(x, y, t) = \frac{v_*^2}{f h_n} T(t) Q(y) \left[-\Pi(x) + \Pi_0 e^{x/R_n} + \frac{\gamma R_n}{2}(e^{(x-l)/R_n} - e^{(-|x+l|)/R_n}) + fT_{\text{int}} Q_y(y) R_n^2 \left(\Pi_x + \frac{\gamma}{2}(-2e^{x/R_n} + e^{(x-l)/R_n} - \text{sgn}(x + l) e^{(-|x+l|)/R_n}) \right) \right], \quad (35)$$

$$v_n(x, y, t) = \frac{v_*^2}{h_n} \left(\lambda_n \Lambda_n(y, t)[\Pi_0 e^{x/R_n} - \gamma R_n(e^{x/R_n} - e^{(x-l)/R_n}) + T_{\text{int}}(t) Q(y) \gamma R_n (2e^{x/R_n} - e^{(x-l)/R_n} - e^{(-|x+l|)/R_n})] \right), \quad (36)$$

$$p_n(x, y, t) = \frac{v_*^2}{h_n} \left[\Lambda_n(y, t)[-\Pi_0 e^{x/R_n} + \gamma R_n(e^{x/R_n} - e^{(x-l)/R_n})] + fQ(y) T_{\text{int}}(t) R_n^2 \left(\Pi_x(x) + \frac{\gamma}{2}(-2e^{x/R_n} + e^{(x-l)/R_n} - \text{sgn}(x + l) e^{(-|x+l|)R_n}) \right) \right]. \quad (37)$$

The complete solution follows after summation over all vertical eigenfunctions, $F_n(z)$, according to (7).

The vertical velocity is determined by the pressure according to

$$w = -\frac{1}{N^2} \left(\frac{\partial}{\partial t} + r \right) p_z.$$

With (37) we find explicitly

$$w(x, y, z, t) = -v_*^2 \sum_{n=1}^{\infty} \frac{F_n'(z)}{N^2 h_n} \left[\left(\frac{\partial}{\partial t} + r \right) \Lambda_n(y, t)(-\Pi_0 e^{x/R_n} + \gamma R_n(e^{x/R_n} - e^{(x-l)/R_n})) + fQ(y) T(t) R_n^2 \left(\Pi_x(x) + \frac{\gamma}{2}[2e^{x/R_n} - w^{(x-l)/R_n} - \text{sgn}(x + l) e^{(-|x+l|)/R_n}] \right) \right], \quad (38)$$

where, from (32) and (34), it follows that

$$\left(\frac{\partial}{\partial t} + r \right) \Lambda_n(y, t) = irI_n(y, ir) + \frac{f_{\text{sc}}}{2}[(i\omega_0 + r) I_n(y, -\omega_0 + ir) e^{-i\omega_0 t} + (i\omega_0 - r) I_n(y, \omega_0 + ir) e^{i\omega_0 t}]. \quad (39)$$

In (38) the very small contribution of the barotropic mode, which is scaled by a factor $v_*/\sqrt{gH}$, was omitted.

The coefficients $w_n(x, y, t)$ are defined by

$$w(x, y, t) = \sum_{n=1}^{\infty} \sin\left(\frac{n\pi}{H} z \right) w_n(x, y, t)$$

and (38) in an obvious manner. In order to visualize the results we have to perform the mode sums numerically. We choose 100 vertical modes although the results are virtually the same as for 50 modes. The involved parameters are $v_*^2 = 1.2$ cm^2 s^{-2}, $H = 1$ km, $H_{\text{mix}} = 60$ m, $R_1 = 55$ km, $f = 6 \times 10^{-5}$ s^{-1}, $N = 10^{-3}$ s^{-1}, $r = 0.02f$, $l = R_1$, $\Pi_0 = 0.75$, $\Pi_\infty = 1$, and $f_{\text{sc}} = 0.2$.

The simple linear friction r sets a timescale but is not

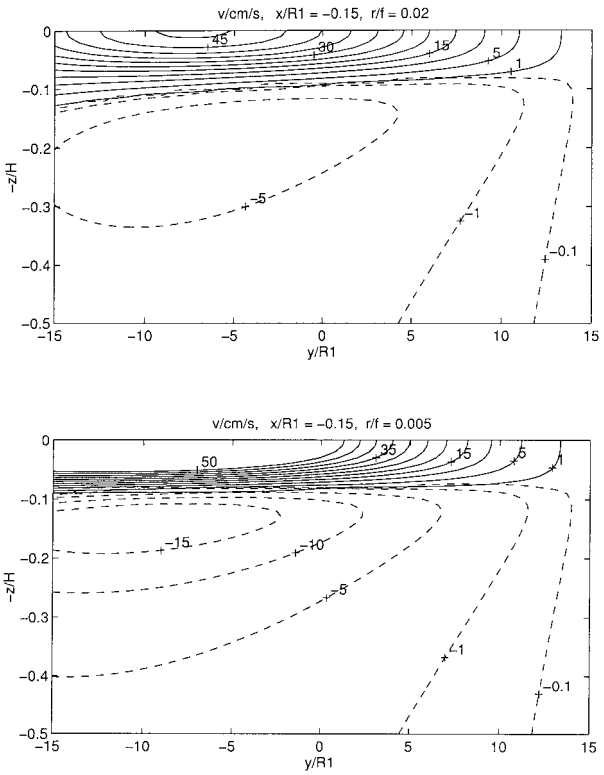

FIG. 4. The steady alongshore flow for finite $r = 0.02f$ (top) and small friction $r = 0.005f$ (bottom). The positive contours (solid) are 1, 5, and then progressing in intervals of 5 cm s^{-1}. The negative contours (dashed) are -0.1, -1, and then progressing in intervals of -5 cm s^{-1}.

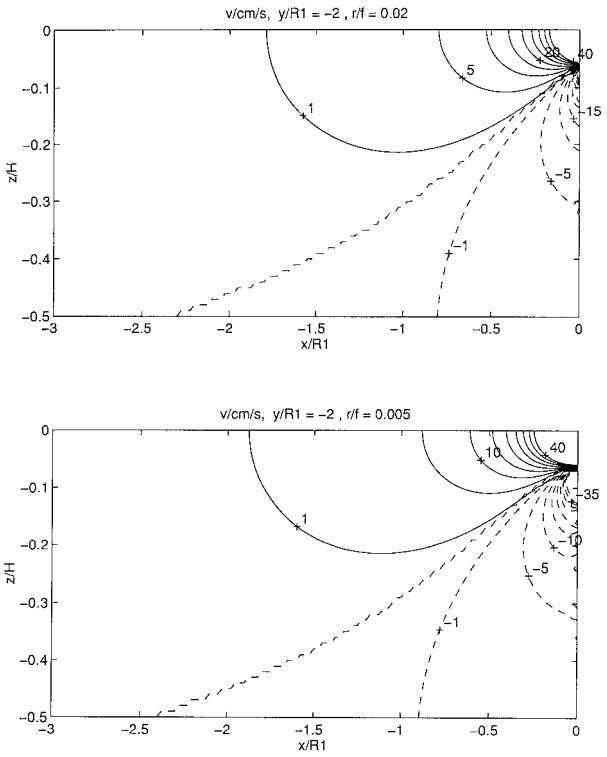

FIG. 5. Cross sections of the steady alongshore flows for $r = 0.02f$ (top) and $r = 0.005f$ (bottom) at $y = -2R_1$. The contour intervals are ± 1, ± 5, and then progressing in steps of ± 5 cm s^{-1}.

scale selective with respect to the spatial scales. In order to compare the order of magnitude of r with an eddy viscosity approach we may consider a coastal jet with $u \sim \exp(x/R_n)$. Comparing ru with

$$A_H \frac{\partial^2}{\partial x^2} u \sim \frac{A_H}{R_n^2} u,$$

we find as a rough estimate $r \sim A_H/R_1^2$. Thus the choice of $r = 0.02f$ corresponds to $A_H = 3.3 \times 10^6$ cm^2 s^{-1}, which is a reasonable order of magnitude for numerical shelf ocean models.

4. Discussion

The oceanic response is composed of the steady-state contributions, the part due to the seasonal cycle controlled by f_{sc}, and by the wind stress curl, controlled by γ.

We start the discussion of the results with the case of a nonrotational stationary wind, that is, $\gamma = 0$, implying $\Pi_\infty = \Pi_0 = 1$, and $f_{sc} = 0$. This corresponds to the case where the wind was switched on at $t \to -\infty$. The alongshore flow consists of a directly wind driven coastal jet arrested by wave processes. Since we ignore planetary Rossby waves and continental shelf waves, the adjustment is established through Kelvin waves. The coastal flow increases from north to south within the wind band. This is because the weak wind, Y, in the ramp region (see Fig. 3) forces a weak local coastal jet and southward propagating Kelvin waves strengthen the coastal current to the south in an inviscid ocean. In other words, the Kelvin waves stop the acceleration of the coastal jet later in the middle and southern parts of the wind band. In the viscid ocean the shape of the stationary coastal current is controlled by the propagation distances of the Kelvin waves, which depend on the friction parameter r and modenumber n. Note the exponential $\exp[i\overline{\omega}\lambda_n(a - y)]$ in (32) becomes

$$\exp[-r\lambda_n(a - y)] = \exp\left(-\frac{r}{f}\frac{(a - y)}{R_n}\right),$$

where fR_n/r is the e-folding scale of the nth-mode Kelvin wave. For $r = 0.02f$ the e-folding scale of the first mode Kelvin wave, $n = 1$, is $fR_1/r = 50R_1 = 2750$ km and $fR_{10}/r = 5R_1 = 275$ km for the mode $n = 10$; that is, the higher modes are damped more than the lower ones.

In Fig. 4 the steady alongshore flows are shown for $r = 0.02f$ (top). A reduction of the friction parameter, $r = 0.005f$, increases the speeds due to the reduced damping and the longer propagation distances of the Kelvin waves (Fig. 4, bottom). The alongshore current

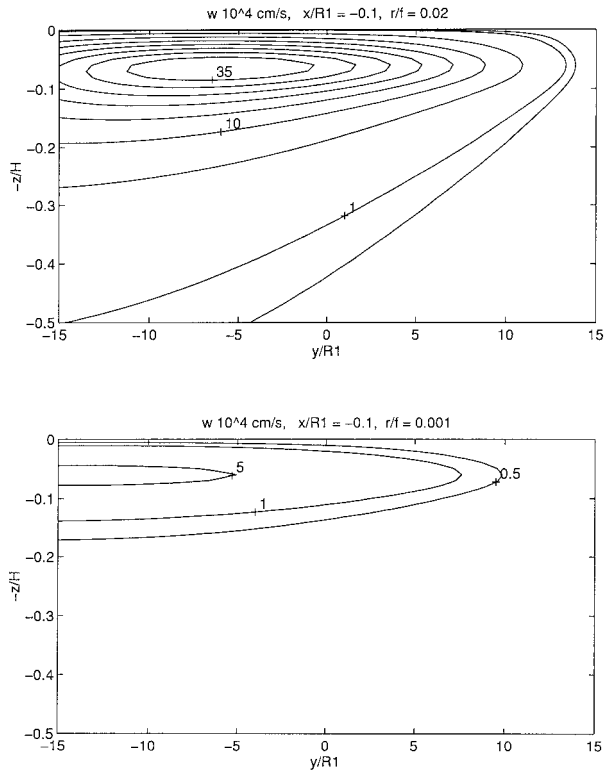

FIG. 6. The steady vertical flows for $r = 0.02f$ (top) and $r = 0.001f$ (bottom). For very small friction the upwelling tends to zero. The contour intervals are 0.5, 1, 5, and then progressing in steps of 5 cm s^{-1}.

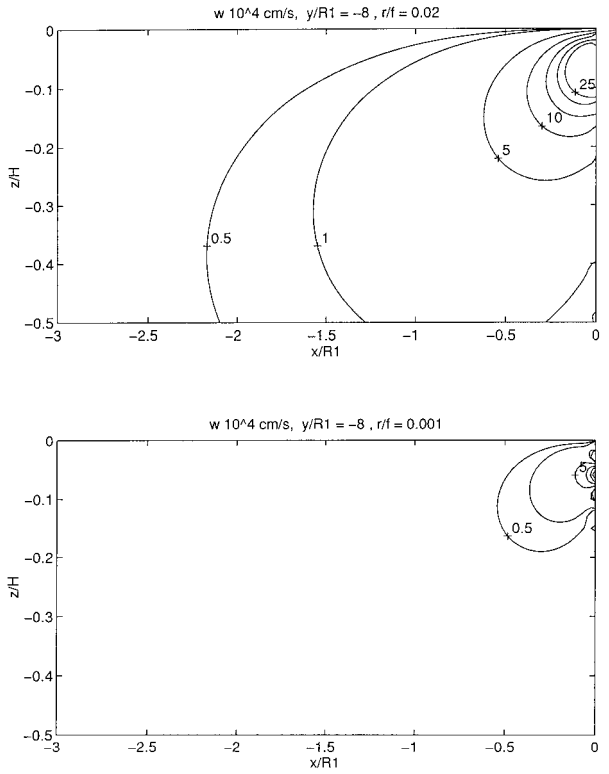

FIG. 7. Cross sections of the steady vertical flows for $r = 0.02f$ (top) and $r = 0.001f$ (bottom) at $y = -8R_1$. The contour intervals are as in Fig. 6.

is not very sensitive to changes of the friction parameter r. Differences occur mainly in the southern part of the wind band where the surface flow and the undercurrent increase with decreasing friction. Corresponding cross sections of the flow are shown in Fig. 5. The enhancement of the flow due to the reduction of friction is located near the coastal boundary.

In the steady-state case the upwelling consists of local Ekman upwelling and the reduction due to the Kelvin waves. Steady upwelling is only possible for nonzero friction, which limits the propagation distance of the Kelvin waves, in particular for the higher modes. The decrease of the steady vertical current due to a reduction of the friction is illustrated in Fig. 6, where the steady vertical currents parallel to the coast are shown for finite friction, $r = 0.02f$ (top), and small friction, $r = 0.001f$ (bottom). The corresponding cross sections of the vertical velocities at $y = -8R_1$ are shown in Fig. 7.

Next we look at the effects of a nonzero wind stress curl; that is, $f_{sc} = 0$ and $\gamma \neq 0$. The wind stress curl, given by the profile $\Pi(x)$, implies a divergence of the Ekman transport. The associated upwelling is centered $x = -l$. Seaward of this line a downwind surface current is generated while in the coastal strip, where the wind weakens, a countercurrent emerges. Since, contrary to a coastal boundary, the wind stress curl does not provide a waveguide mechanism, the magnitude of the current system is rather sensitive to the friction parameter. This is quite similar to the oceanic response in the marginal ice zone, where wind stress variations due to changes of the drag coefficient can generate piecewise linear wind stress profiles (see Fennel and Johannessen 1997).

The southward countercurrent reduces the equatorward coastal flow. In the northern part of the wind band, where the coastal flow is weak relative to the middle and southern part of the wind band, the countercurrent can overcompensate the coastal current. Hence, a poleward coastal flow exist in the northernmost part of the forcing area (Fig. 8, top). A reduction of friction enhances the role of the countercurrent and the poleward coastal flow occupies a wider area of the wind band, Fig. 8 (bottom). The corresponding cross-shore sections are shown in Fig. 9 for $y = -2R_1$.

The contribution to the vertical velocity forced by the wind stress curl is independent of friction. This contribution decreases the resulting upwelling in the southern part of the wind band, as shown in Fig. 10. Note that in this case the wind is reduced by 25% near the coast due to the shape of the wind profile $\Pi(x)$. Thus the pattern of coastal upwelling is affected by wind stress curl. The corresponding cross-shore sections are shown in Fig. 11.

Next we consider the effect of the seasonal cycle of

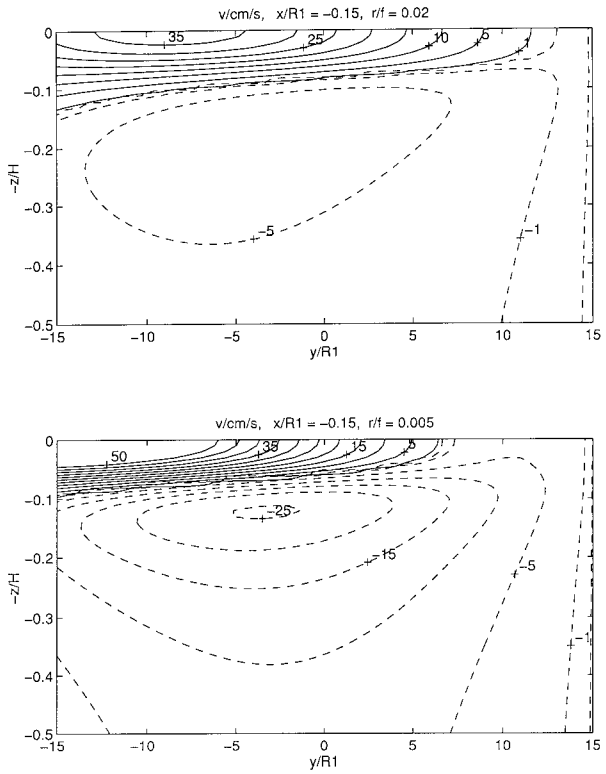

FIG. 8. The steady alongshore flows for a nonzero wind stress curl for $r = 0.02f$ (top) and $r = 0.005f$ (bottom). A reduction of the friction strengthens the role of the countercurrent (bottom). The contour intervals are as in Fig. 4.

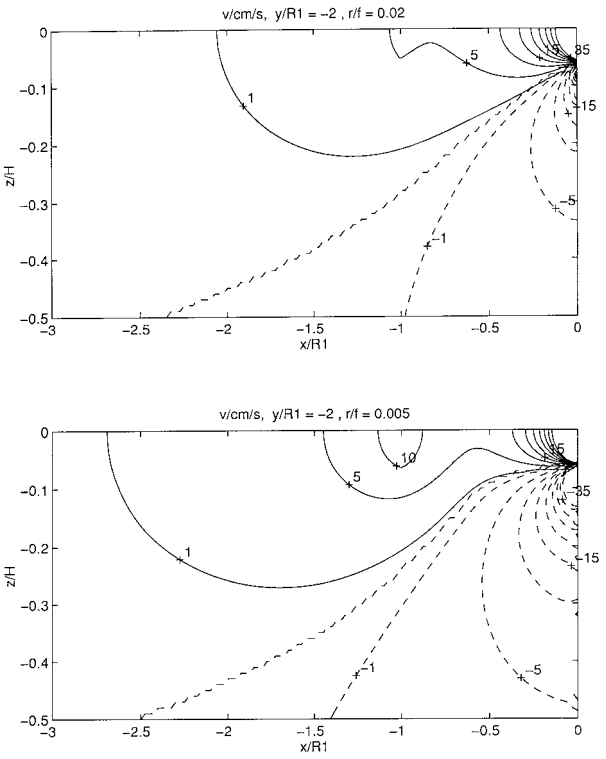

FIG. 9. Cross sections of the steady alongshore flows for a nonzero wind stress curl for $r = 0.02f$ (top) and $r = 0.005f$ (bottom) at $y = -2R_1$. The contour intervals are ± 1, ± 5, and then progressing in steps of ± 5 cm s^{-1}.

the wind on the vertical flow. We start with $f_{sc} \neq 0$ and $\gamma = 0$. The seasonal variation of the wind modifies the stationary signal. For small values of the friction parameter the steady signal tends to zero due to the effect of Kelvin waves, as mentioned above. The oscillatory part of the wind drives local Ekman upwelling and downwelling and generates Kelvin waves, which are associated with downwelling and upwelling, respectively, and propagate southward through the wind band.

For example, the positive (northward) half-wave of the wind oscillation drives coastal Ekman upwelling, which is reduced by downwelling Kelvin waves until the wind assumes the maximum value. After the maximum of the wind oscillation is reached, the downwelling Kelvin waves overshoot the Ekman upwelling and the resulting vertical flow is negative. For the negative (southward) half-wave of the wind oscillation the response is analogous but with opposite sign. The vertical current is out of phase with the wind variation (Fig. 3, top) by $\pi/2$. This is shown in Fig. 12 (top) by means of alongshore-time plot of the first mode vertical velocity, w_1.

For finite friction the Kelvin waves are damped and do not cancel the steady Ekman upwelling. The response of the vertical flow to the seasonal variations of the wind is now dominated by the Ekman upwelling and downwelling because of the reduced effect of the Kelvin waves. The resulting upwelling signal is almost in phase with the wind variations (Fig. 12, bottom).

In the case of a nonzero wind stress curl, $\gamma \neq 0$, there is a further source of upwelling independent of friction. This upwelling signal is not affected by Kelvin waves and has the same alongshore structure as the wind field [see Eq. (38)]. Therefore, the resulting upwelling decreases near the southern edge of the wind band, as shown in Fig. 13 (bottom). Owing to the wind-stress curl contribution the resulting upwelling is almost in phase with the wind, even in the small friction limit (see Fig. 13, top). In Figs. 12 and 13 the first mode, w_1, is shown. The behavior of the first few modes, which dominate the resulting signals, is quite similar as w_1.

For nonzero f_{sc} and γ, the current system, which is composed of the coastal currents and the flows in response to the wind stress curl, varies with time. Alongshore sections of the time-dependent alongshore currents are shown in Fig. 14 for January and July. Owing to the wind maximum in austral summer and the minimum in austral winter, both the surface current and the undercurrent are significantly stronger in January than in July. The poleward surface flow near the northern boundary of the wind band has an alongshore scale of a few first-mode Rossby radii and shows only little seasonal variation.

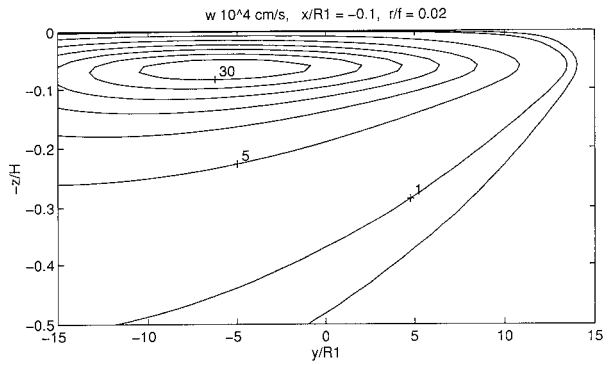

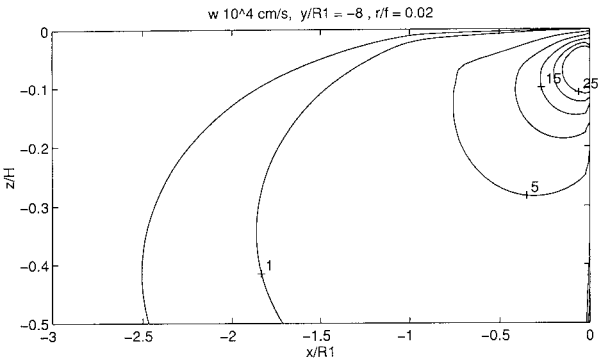

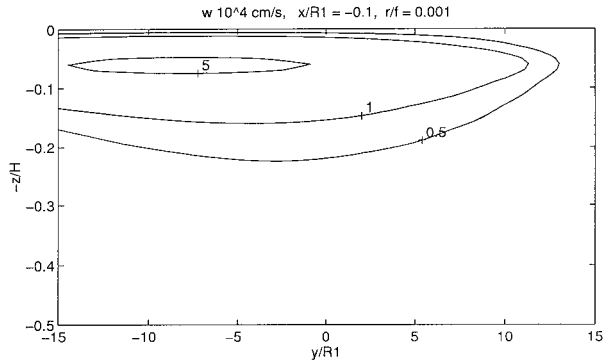

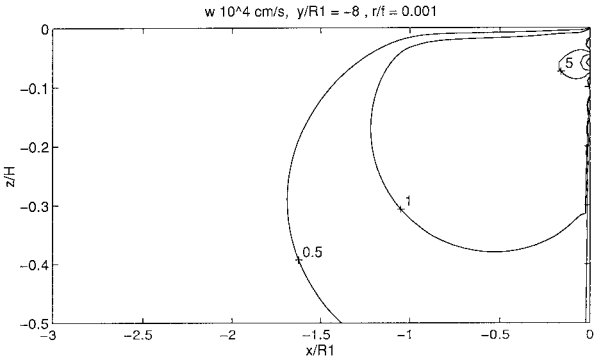

FIG. 10. The steady vertical flows for a nonzero wind stress curl for $r = 0.02f$ (top) and $r = 0.001f$ (bottom). The contour intervals are as in Fig. 6.

FIG. 11. Cross sections of the steady vertical flows for a nonzero wind stress curl for $r = 0.02f$ (top) and $r = 0.001f$ (bottom) at $y = -8R_1$. The contour intervals are as in Fig. 6.

Sections of the alongshore current normal to the coast are shown in Fig. 15 for January and Fig. 16 for July, for different locations: $y/R_1 = 10$, $y/R_1 = 0$, and $y/R_1 = -10$. The alongshore currents broaden toward the southern border of the wind band.

Alongshore sections of the vertical velocities are shown in Fig. 17 for January and July. Cross-shore sections of the vertical velocity at different locations are shown in Figs. 18 and 19 for January and July. Owing to the seasonal variation of the wind the upwelling is stronger and broader in summer (January) than in winter (July).

At the southern border of the wind band the currents are rather strong owing to the Kelvin waves, which have to propagate longer distances before they can arrest the coastal jet. The coastal flows and the upwelling will be exported southward by a second set of Kelvin waves. The export of the coastal current and the upwelling outside the forcing area along a straight coast is shown in Fig. 20 and Fig. 21 for January and July. For a curved coast the Kelvin waves follow the coastline (Clarke 1977) and may propagate around the southern tip of Africa. Thus the theory implies that a remotely forced westward coastal jet may be generated south of Africa, which transports Agulhas waters into the Benguela upwelling system off southwest Africa.

South of Africa the Agulhas has features of a free inertial jet that starts to meander and decays into eddies and rings in the Agulhas retroflection zone (Lutjeharms 1996). Since Kelvin waves propagate with the coast to the left there is, from the theoretical viewpoint, no property of the Agulhas that forces the current to follow the coastline off southwest Africa. Hence the theory suggests that the coastal jet, which is exported outside the Benguela upwelling system, provides a dynamic linkage between the westward Agulhas off the southern coast of Africa and the northward coastal current of the Benguela upwelling system.

5. Summary and conclusions

Owing to Kelvin waves, which are generated continously in response to the changing wind forcing, the signals of the coastal jet propagate poleward leaving a relatively weak coastal jet in the northern part of the area. Due to the Kelvin waves the coastal jet and upwelling are stronger near the southern border of the wind band. The upwelling maximum is shifted somewhat southward of the location of the wind maximum. This seems to be in accordance with the strong upwelling observed off Lüderitz, Namibia.

The wind stress curl, due to the decrease of the alongshore wind near the coast, appears to be an important dynamic feature in shaping the upwelling system. It

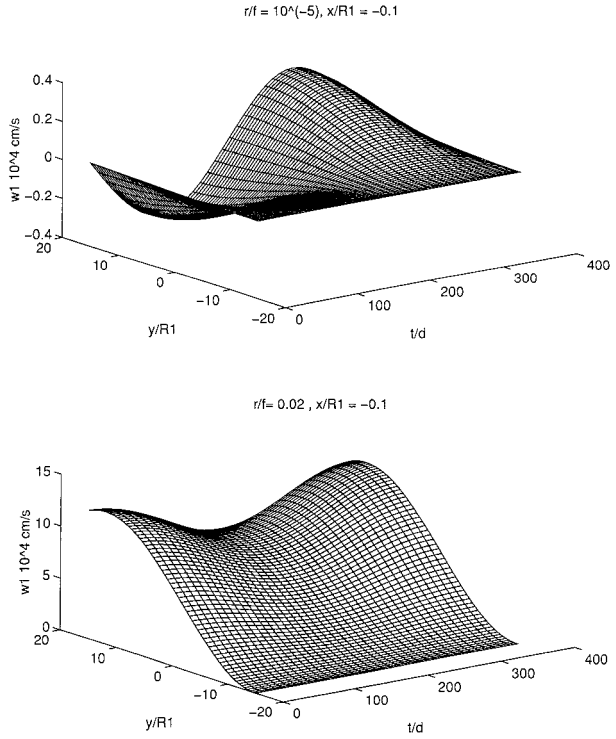

FIG. 12. Alongshore–time view of the first mode vertical velocity for zero wind stress curl and for a very small ($r = 10^{-5}f$) (top) and finite friction parameter ($r = 0.02f$) (bottom).

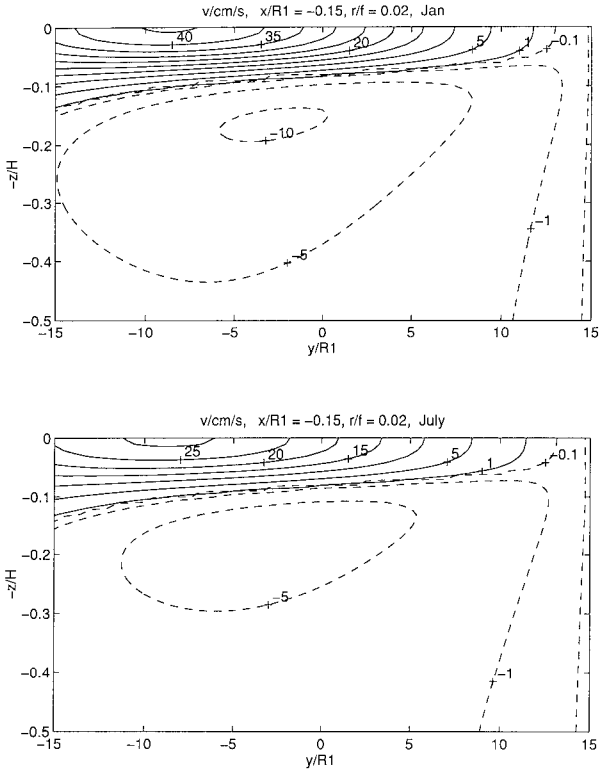

FIG. 14. Yearly variation of the alongshore current shown in terms of the extremes in summer and winter. Shown are alongshore sections for January (top) and July (bottom). The positive contours (solid) are 1, 5, and then intervals of 5 cm s^{-1}. The negative contours (dashed) are -0.1, -1, and then progressing in intervals of -5 cm s^{-1}.

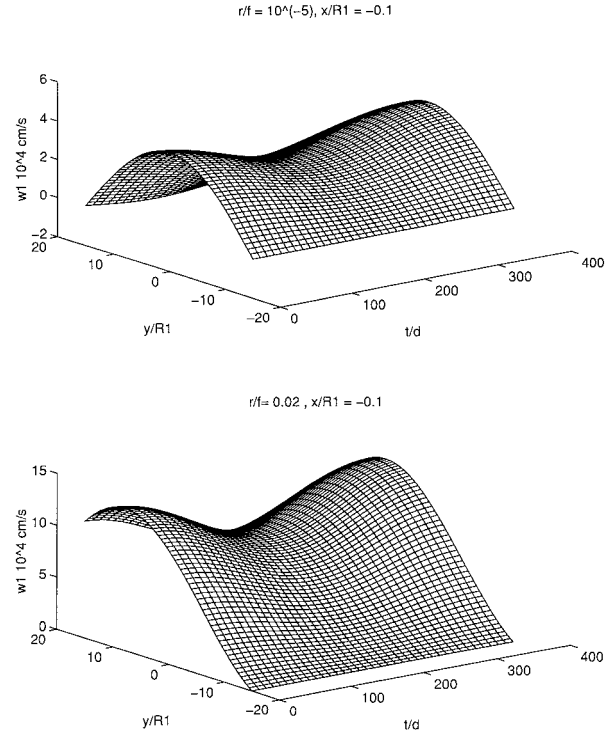

FIG. 13. Alongshore–time plot of the first mode vertical velocity for nonzero wind stress curl and with very small ($r = 10^{-5}f$) (top) and finite friction ($r = 0.02f$) (bottom).

produces a secondary divergence of the offshore Ekman transport and forces upwelling and a downwind surface flow in the offshore area ($x < -l$) where the wind reaches its maximun and a countercurrent in the coastal strip ($-l < x < 0$).

The countercurrent reduces the equatorward coastal jet. Near the northern border of the wind band, where the coastal current is weak due to the effect of Kelvin waves, the counterflow exceeds the coastal jet and produces even a poleward surface flow. Thus the model study shows that the poleward surface flow can be locally forced. It is not necessarily driven remotely by equatorial Kelvin waves. A similar mechanism was studied by McCreary et al. (1987) to explain the occurrence of the poleward coastal surface flow in the California Current system.

The response to the wind curl is not affected by Kelvin waves because the wind variation provides no wave guide at the coastal boundary. Thus the horizontal component of this flow is completely balanced by friction, while the vertical component is independent of the friction parameter. Both components have the same alongshore shape as the wind field.

Near the southern border of the wind band the vertical component is somewhat reduced. This is due to the con-

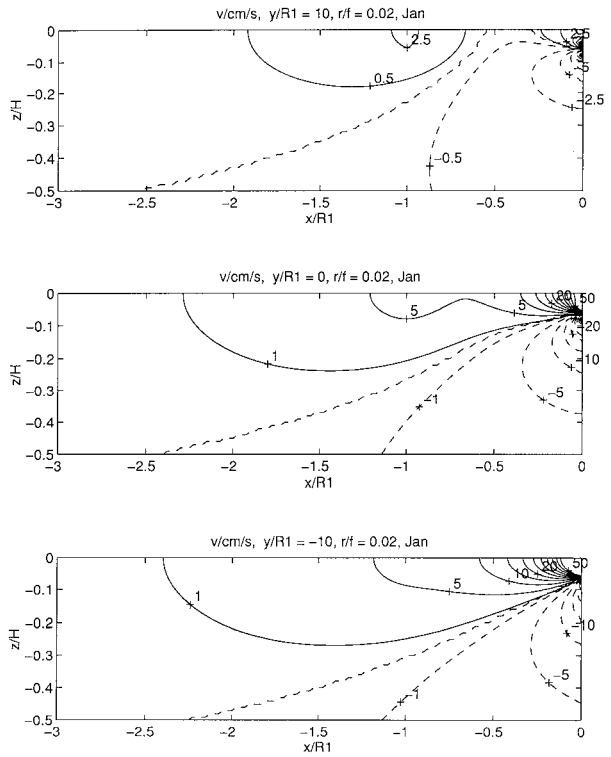

FIG. 15. Cross-shore sections of the alongshore current at three locations for January. For $y = 10R_1$ (top) the contour intervals are ± 0.5, ± 2.5, and then progressing in steps of ± 2, 5 cm s^{-1}. For $y = 0$ (middle) and $y = -10\ R_1$ (bottom) the contour intervals are ± 1, ± 5, and then progressing in steps of ± 5 cm s^{-1}. Negative contours are dashed.

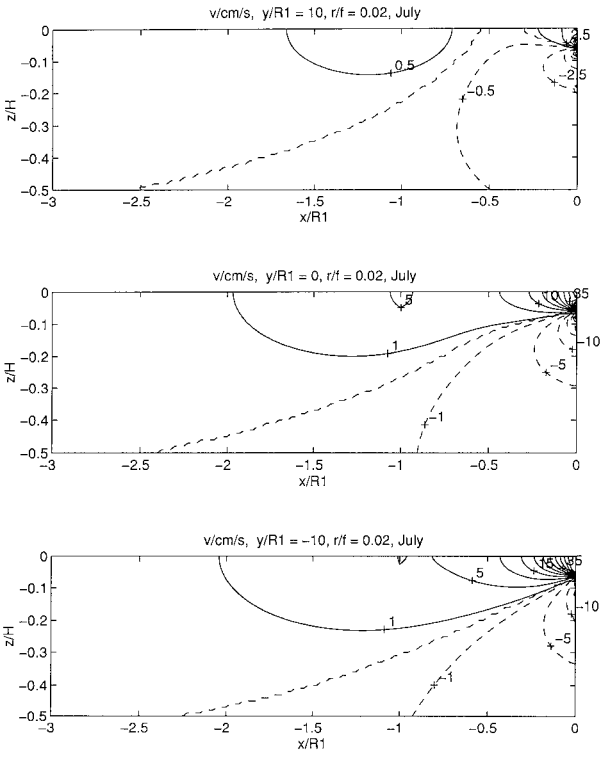

FIG. 16. Same as Fig. 15 but for July.

tribution of the wind stress curl. Without this contribution the upwelling would be higher in the south due to the Kelvin waves.

At the southern border of the wind band a second set of Kelvin waves exports the coastal currents and the upwelling along the coastline. The exported coastal jet flows westward off the southern coast of Africa and can drain Agulhas waters into the upwelling area off southwest Africa. This suggests a dynamic linkage between the the Benguela upwelling system and the Agulhas.

The theory is strongly simplified and therefore has several deficiencies, which is the price to obtain an analytically tractable set of equations. The wind field is strongly idealized and the differences in the seasonal cycles in the southern and northern part off southwest Africa are not resolved. The theory is linear and, therefore, formation of fronts and instabilities are not considered. The coast is replaced by a straight vertical wall and the shelf was negelected. This implies that the only boundary waves seen by the model are Kelvin waves. Moreover the β effect, which gives rise to a shedding of Rossby waves, was excluded.

Nevertheless, the model is able to simulate major features of the circulation, suggesting that it contains much of the fundamental dynamics involved in the Benguela

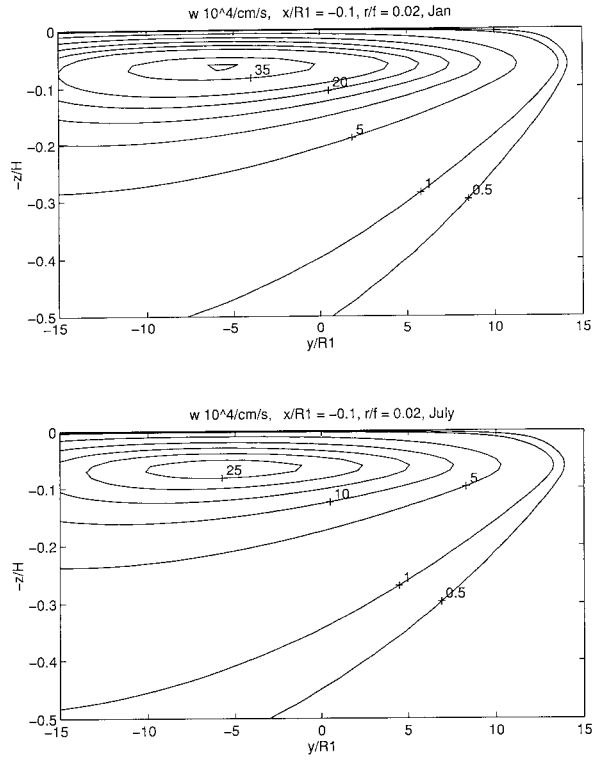

FIG. 17. Yearly variation of the vertical velocity shown in terms of the extremes in austral summer and winter. Shown are alongshore sections for January (top) and July (bottom). The contour intervals are 0.5, 1, 5, and then progressing in steps of 5 cm s^{-1}.

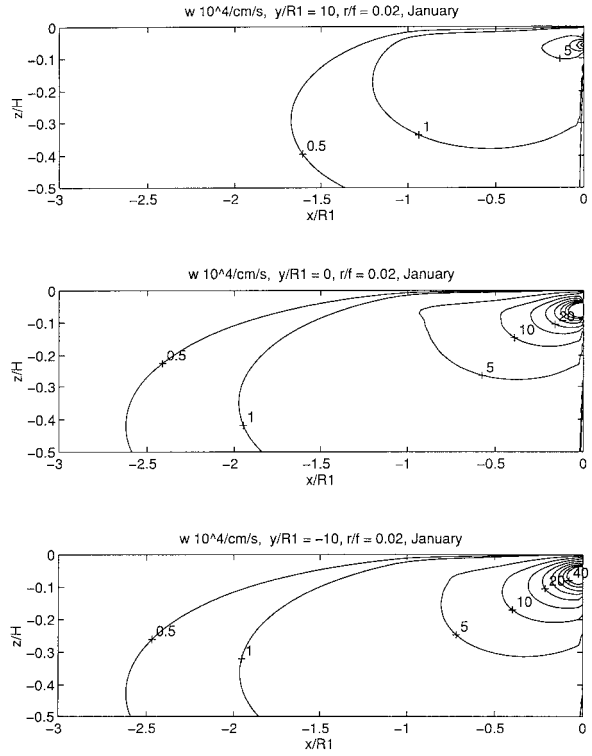

FIG. 18. Cross-shore sections of the vertical velocity at three locations for January. The contour intervals are 0.5, 1, 5, and then progressing in steps of 5 cm s^{-1}.

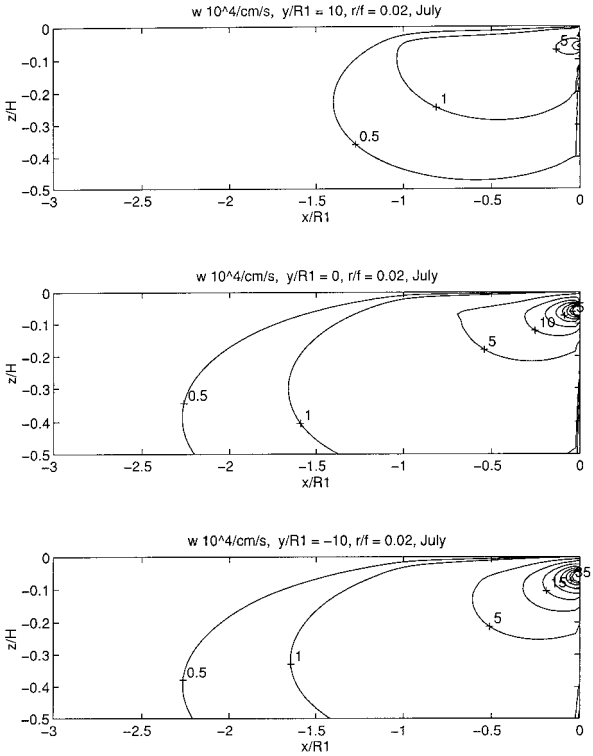

FIG. 19. Same as Fig. 18 but for July.

upwelling system. The findings may provide some guidance for a discussion of the results of ocean general circulation models of this area.

Acknowledgments. The author thanks two anonymous referees for critical and helpful comments on an earlier version of the manuscript.

APPENDIX

Convolution Integrals

The calculation of the convolution integrals of the type of (19) amounts to estimating the integral

$$G_n * \Pi = \int_{-\infty}^{0} dx'\ G_n(x; x')\Pi(x'), \qquad \text{(A1)}$$

where G_n is given by (15) and Π by (22). Rewriting (14) as

$$G_n(x; x') = \frac{1}{\alpha_n^2}\left(-\delta(x - x') + \frac{d^2}{dx'^2}G_n(x; x')\right),$$

and inserting this in (A1), we can solve the integral easily by integration by parts:

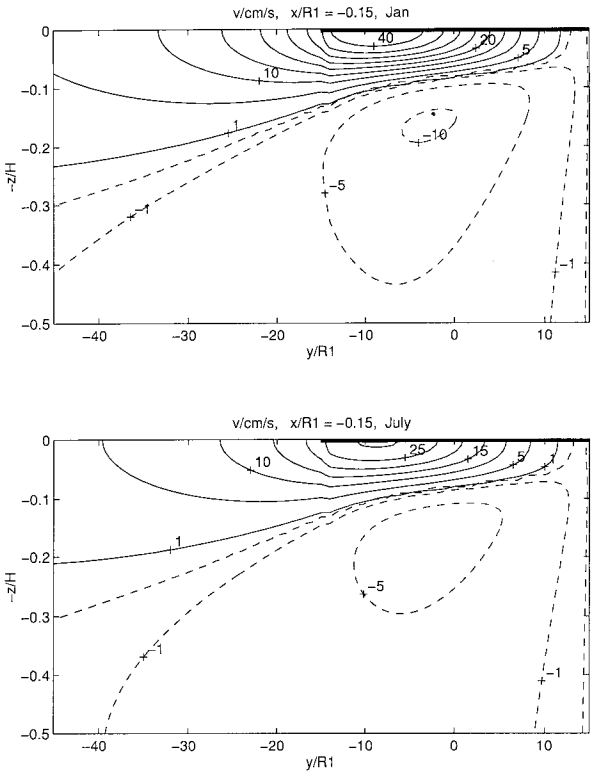

FIG. 20. Same as Fig. 14 but extended to the south to illustrate the southward export of the coastal current. The thick line indicates the forcing area.

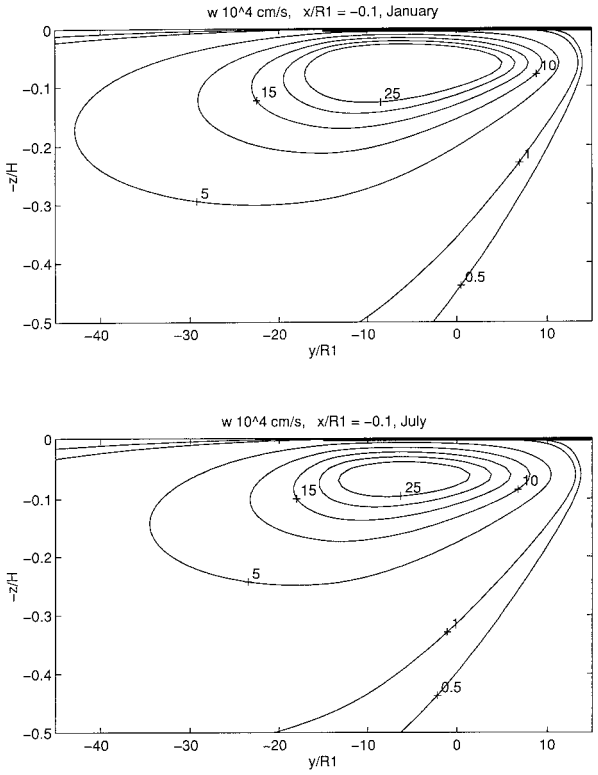

FIG. 21. Same as Fig. 17 but extended to the south to illustrate the southward export of upwelling. The thick line indicates the forcing area.

$$G_n * \Pi = \frac{1}{\alpha_n^2}(\Pi_0 e^{\alpha_n x} - \Pi(x) + \gamma G_n(x; l)).$$

In a similar manner we find

$$G_n * \Pi_{x'} = \frac{1}{\alpha_n^2}(-\Pi_x(x) + \gamma(G_{nx'}(x; 0) - G_{nx'}(x; l))$$

and

$$G_{nx} * \Pi = \frac{1}{\alpha_n^2}(\alpha_n \Pi_0 e^{\alpha_n x} - \Pi_x(x) + \gamma G_{nx}(x; l)).$$

REFERENCES

Bakun, A., and C. S. Nelson, 1991: The seasonal cycle of wind-stress curl in the sub-tropical eastern boundary current regions. *J. Phys. Oceanogr.,* **21,** 1815–1834.

Bang, N. D., 1973: Characteristics of an intense ocean frontal system in the upwell regime west of Cape Town. *Tellus,* **25,** 256–265.

Boyd, A. J., 1987: The oceanography of the Namibian shelf. Ph.D. thesis, University of Cape Town, 190 pp.

Clarke, A. J., 1977: Wind-forced linear and nonlinear Kelvin waves along an irregular coastline. *J. Fluid Mech.,* **83,** 337–348.

Emery, W. J., W. G. Lee, and L. Maagard, 1984: Geographic and seasonal distributions of the Brunt–Väisälä frequency and Rossby radii in the North Pacific and the North Atlantic. *J. Phys. Oceanogr.,* **14,** 294–317.

Fennel, W., 1988: Analytical theory of the steady-state coastal ocean and equatorial ocean. *J. Phys. Oceanogr.,* **18,** 834–850.

——, and O. M. Johannessen, 1998: Wind forced oceanic responses near ice edges revisited. *J. Mar. Syst.,* **14,** 57–79.

Garsoli, S. L., and A. L. Gordon, 1996: Origins and variability of the Benguela Current. *J. Geophys. Res.,* **101,** 987–906.

Lutjeharms, J. R. E., 1996: The exchange of water between the South Indian and the South Atlantic Oceans. *The South Atlantic: Present and Past Circulation,* G. Wefer, W. H. Berger, G. Siedler, and D. J. Webb, Eds., Springer-Verlag, 125–162.

McCreary, J. P., 1981: A linear stratified ocean model of the coastal undercurrent. *Philos. Trans. Roy. Soc. London, Series A,* **302,** 385–413.

——, P. K. Kundu, and S. Y. Chao, 1987: On the dynamics of the California Current system. *J. Mar. Res.,* **45,** 1–32.

Nelson, G., and L. Hutchings, 1983: The Benguela upwelling area. *Progress in Oceanography,* Vol. 12, Pergamon, 333–356.

Schumann, E. H., L. A. Perrins, and I. T. Hunter, 1982: Upwelling along the south coast of the Cape Providence, South Africa. *South Africa J. Sci.,* **78,** 238–242.

Shannon, L. V., 1985: The Benguela Ecosystem, Part I: Evolution of the Benguela, physical features and processes. *Oceanogr. Mar. Biol.,* **23,** 105–182.

——, and G. Nelson, 1996: The Benguela: Large-scale features and process and system variability. *The South Atlantic: Present and Past Circulation,* G. Wefer, W. H. Berger, G. Siedler, and D. J. Webb, Eds., Springer-Verlag, 162–210.

——, S. A. Mostert, N. M. Walters, and F. P. Anderson, 1983: Chlorophyll concentrations in the southern Benguela Current region as determined by satellite (Nimbus-7 coastal zone colour scanner). *J. Plankton Res.,* **5,** 565–583.

——, J. J. Agenbag, N. D. Walker, and J. R. E. Lutjeharms, 1990: A major perturbation in the Agulhas retroflection area in 1986. *Deep-Sea Res.,* **37,** 493–512.

Yamagata, T., and S. Iizuka, 1995: Simulation of the tropical thermal domes in the Atlantic: A seasonal cycle. *J. Phys. Oceanogr.,* **25,** 2129–2140.